ZIBELINE INTERNATIONAL™ PUBLISHING

ISSN: 2521-0890 (Print)
ISSN: 2521-0491 (Online)
CODEN: GBEEB6

Geological Behavior (GBR)

DOI: http://doi.org/10.26480/gbr.02.2025.100.107

RESEARCH ARTICLE

INTEGRATING SEISMIC REFRACTION IMAGING AND ELECTRICAL RESISTIVITY TOMOGRAPHY TO DELINEATE AQUIFER ZONES IN SELECTED AREAS AROUND MARABAN RIDO, KADUNA

Halima Haruna[a]*, Abdullah Musa Ali[b] .

[a]*Department of Mineral and Petroleum Resources Engineering, College of Engineering, Kaduna polytechnic, Kaduna*
[b]*Department of Geology, Bayero University Kano (BUK), Kano*
**Corresponding Author Email: halimajubrinharuna@gmail.com*

ARTICLE DETAILS

Article History:

Received 15 July 2025
Revised 13 August 2025
Accepted 18 September 2025
Available online 08 October 2025

ABSTRACT

This research is aimed at integrating Electrical Resistivity Tomography (ERT) and Seismic Refraction Tomography (SRT) methods to delineate potential aquifer zones in parts of MarabanRido, Kaduna, Northwest, Nigeria. The research area, located in Kaduna South, features a mix of deposits and basement rock formations, making it a challenging region for groundwater exploration. The ERT survey utilized the ABEM Terrameter SAS 4000 with multi-electrode configurations, while the SRT employed a 24-channel ABEM Terraloc Pro2 seismic acquisition system. Data from both methods were processed using advanced software—RES2DINV for ERT and ReflexW for SRT to generate 2D resistivity and velocity models. The topsoil layer exhibits a seismic velocity range of 650 to 800 m/s and a resistivity range of 50 - 400Ωm, overlying a weathered basement with seismic velocity range of 900 to 2000 m/s with resistivity values between 500 and 1000Ωm. A third layer with velocities from 920 to >1384 m/s corresponds to resistivity values of 2058–9486 Ωm, indicative of moderately to highly weathered granite transitioning into fresh basement rock. The average overburden thickness is approximately 8 m, with basement depths around 20 m. The depth ranges and structural patterns interpreted from the ERT data align strongly with the SRT results, confirming the reliability of the integrated geophysical approach. The strong correlation between wave velocity and resistivity distributions allowed for accurate identification of groundwater-bearing zones, particularly within fractured and weathered basement complexes. This integrated method proves to be a reliable tool for hydrogeological investigations in crystalline hard rock terrains, supporting its application in groundwater explanation.

KEYWORDS

Seismic Refraction Tomography, Electrical Resistivity Tomography, Velocity, Aquiferous zone, Crystalline basement rocks

1. INTRODUCTION

MarabanRido is located in the southeastern part of Kaduna State, Nigeria. It has a complex geology, characterized by diverse lithological composition that includes gneisses, granites, migmatite, schist and metavolcanics. The study area predominantly consists of biotite granites with minor amphibolite dykes, quartz vein and quartzofeldspathic intrusions. Some of the associated structures are fractures and join sets. This complexity in geology demands efficient exploration to ensure long-term utilization of groundwater (Ali et al., 2017). Climate change issues and the increasing demand for water in the study area have led to challenges of scarcity and over-extraction. Geophysical techniques, particularly seismic refraction tomography (SRT) and electrical resistivity tomography (ERT) have proven to be highly effective in delineating aquifer zones, offering a non-invasive means of mapping subsurface features (Ali et al., 2017). These methods complement each other, making them especially relevant in areas like MarabanRido, Kaduna South, where complex geological formations are present.

Recent advancements in seismic refraction processing and imaging technologies have increased the accuracy and depth resolution of subsurface profiles with the utilization of seismic methods to map basement layers. (Ismail et al., 2013). SRT is widely used in hydrogeophysical surveys to image the subsurface by recording the velocity of seismic waves as they refract at geological boundaries. The method identifies different layers based on their seismic velocities, which can help distinguish between saturated aquifer zones and impermeable bedrock or consolidated formations. SRT is also valuable for identifying the boundary between overlying sediments and bedrock, as well as for locating fractured zones that might serve as conduits for groundwater (Yadav and Abolfazli, 2017). Lower seismic velocities generally indicate water-saturated layers, making the method suitable for delineating aquifers in areas where groundwater resources are located in fractured or porous formations. Furthermore, SRT is particularly effective in regions with significant geological heterogeneity.

On the other hand, electrical resistivity tomography is a well-established technique for mapping variations in the electrical properties of subsurface materials (Mahmud et al., 2022). It measures the resistivity of different geological layers, with aquifers generally exhibiting low resistivity values due to the presence of water. In contrast, dry, compacted formations, or bedrock tend to have higher resistivity values (Ahzegbobor et al., 2018).In groundwater studies, ERT provides detailed images of subsurface structures, identifying potential aquifer zones and delineating their depth

Quick Response Code	Access this article online	
	Website: www.geologicalbehavior.com	DOI: 10.26480/gbr.02.2025.100.107

Cite The Article: Halima Haruna, Abdullah Musa Ali. (2025). Integrating Seismic Refraction Imaging And Electrical Resistivity Tomography To Delineate Aquifer Zones In Selected Areas Around Maraban Rido, Kaduna. *Geological Behaviour 9(2): 100-107* .

and extent (Griffiths and Barker, 1993). The method helps detect lateral variations in resistivity that indicates different hydrogeological units.

The combined use of seismic refraction tomography and electrical resistivity tomography offers a powerful approach to groundwater exploration. While SRT provides information about the mechanical properties of subsurface materials, ERT focuses on their electrical properties, particularly related to water content. This complementary nature allows for a more detailed and accurate delineation of aquifer zones.Recent research highlights the importance of integrating these methods to overcome the limitations of each technique when used alone (Salako et al., 2018).Studies conducted in similar geological settings have shown that combining SRT and ERT can significantly improve the detection of groundwater-bearing formations (Salako et al., 2018). As a study applied both methods to map aquifers in a fractured basement setting, achieving better resolution of aquifer boundaries compared to using either method individually (Parisa et al., 2021). This integrated approach allows for the identification of both the depth of aquifers and the nature of the geological formations controlling groundwater flow. Integrating seismic refraction and electrical resistivity data offers a synergistic approach to geological mapping, combining the complementary strengths of both methods to enhance the resolution and reliability of subsurface imaging (Ahmed et al., 2014).

The research area, located in Kaduna South, features a mix of deposits and basement rock formations, making it a challenging region for groundwater exploration. The integration of seismic refraction and electrical resistivity methods is particularly suited to this complex geological environment. By combining the mechanical insights from SRT with the electrical properties obtained from ERT, this approach offers a more robust and detailed understanding of subsurface conditions, ensuring better management of groundwater resources in the region.

2. Geology And Hydrogeology Of The Study Area

The area comprises rocks that range in age from Pre-Cambrian to Lower Palaeozoicand Quaternary period.The dominant rock types include the migmatite-gneiss complex and the Older Granites (Fig. 1), which intruded the host gneissic rocks. Much earlier on,four groups of rocks were distinguished for the BasementComplex Terrain in the area (Young, 1962). The first group consists of crystalline basement rocks, comprising gneisses and migmatites with different varieties of the gneisses such as the banded gneiss,granite gneiss, biotite gneiss, hornblende gneiss and ortho-gneiss. The second group includes the metasediments, specifically quartzite. The thirdgroup is the intrusive rock consisting mainly of granites. The fourth group of rock isthe basalt which is Quaternary in age.The reconnaissance field map (Fig. 2) prepared for the study area indicates the predominant presence of migmatite gneiss rocks (Fig. 3(a)). Other observed rocks include pink granitic gneiss rock,biotitegranite, and granite gneiss as shown in figure 3. Extensive in-situ weathering of the Crystalline Basement rocks under tropical conditions has produced a sequence of unconsolidated material (laterites) (Fig. 4) whose thickness and lateral extent vary extensively.

The groundwater aquifers in the area include the softoverburden (weathered overburden aquifer), fractured bedrock, and alluvium aquifers (stream alluvial deposits). This study reported the presence of three hydrogeological unitsin Kaduna state which includes: a modern alluvium of present day river channels andancient alluvium of the Fadama under silts, and abnormally thick regoliths overlyingBasement Complex, Granite and Metasedimentary rocks and fractures in the freshgranitic rocks, regoliths and ancient alluvium underlying basaltic flows (Parkman international and Parkman Nigerian limited, 1997).

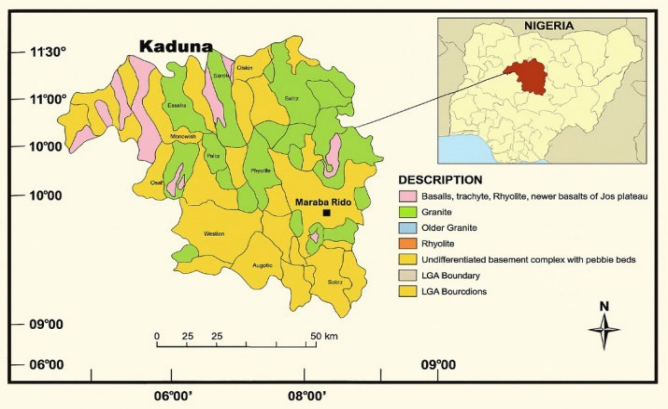

Figure 1: Geological map of Kaduna State indicating the study area (Modified after Fatihu et al., 2021)

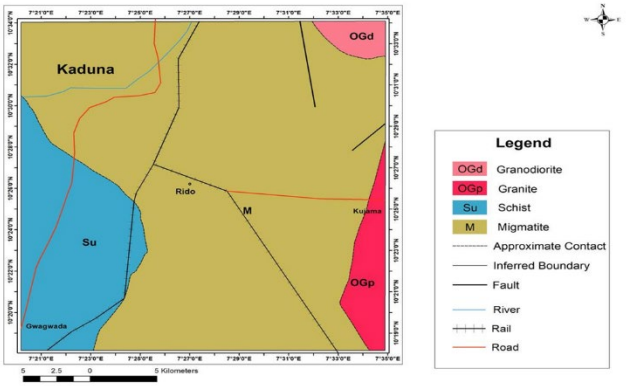

Figure 2: Map Showing Rocks With Associated Geological Structures

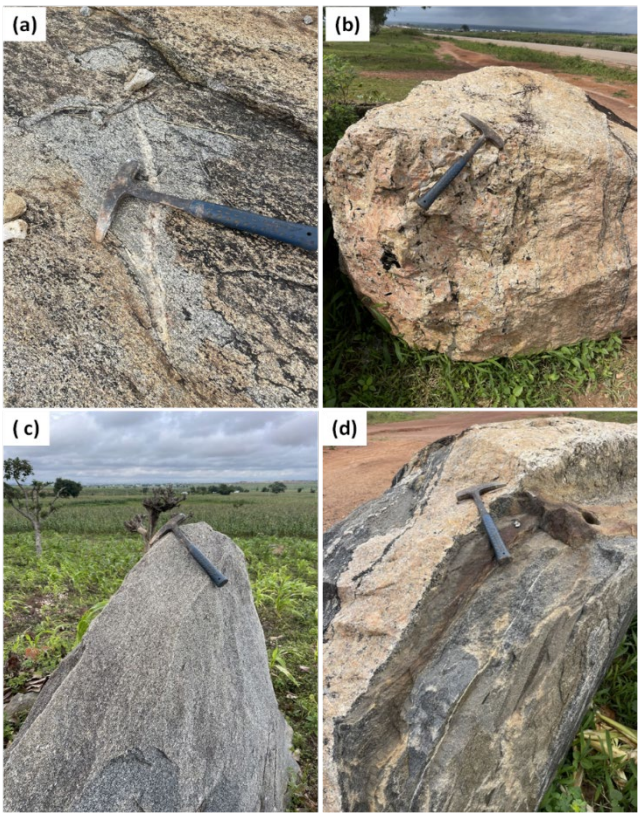

Figure 3: (a) migmatite gneiss complex with granitic intrusion (b) pink granitic gneiss rock (c) biotite granite (d) granite gneiss

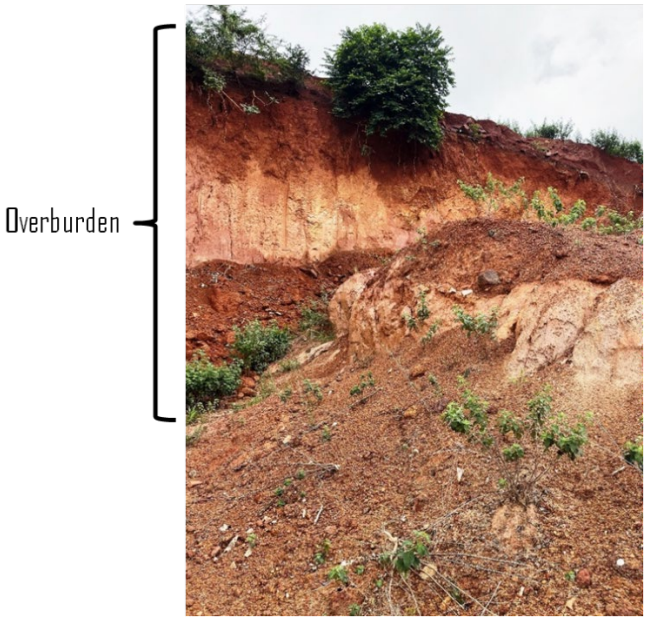

Figure 4: Thick lateritic overburden overlying the crystalline basement

3. Materials And Methods

3.1 Data acquisition and Processing

3.1.2. SRT

The seismic refraction tomography (SRT) survey commenced with a preliminary geological reconnaissance to select appropriate survey lines, considering accessibility, geological diversity, and minimal ambient noise interference. This also ensured effective ground coupling for the geophones. Seismic data were acquired using a 24-channel digital seismograph system (ABEM Terraloc Pro2). The profile extends for a total length of 125 m with inter-geophone spacing of 5 m using 24 geophones. The survey area lies between Latitude 10° 19′ 0″ N to 10° 44′ 57″ N and Longitude 7° 28′ 59″ E to 7° 44′ 31″ E.To give good information for interpretation, no of samples was 4096 while sampling interval used was 200 microseconds which gives a total record length of 819.2 m for P-waves. A 7.26-kg sledgehammer striking a 38 cm diameter and 6 cm thick steel plate was used as the seismic energy source. Eleven shot points were strategically located along the profile at positions: -10, -5, 0, 5, 50, 55, 60, 110, 115, 120, and 125 meters. To enhance the signal-to-noise ratio, each P-wave signal was stacked five times. During the data acquisition phase, first-arrival travel times of refracted seismic waves were recorded across all channels. The data were sampled at 200 microseconds with a total of 4096 samples per shot, resulting in a record length of 819.2 milliseconds per trace. Google map showing the profile lines are presented in figure 5.

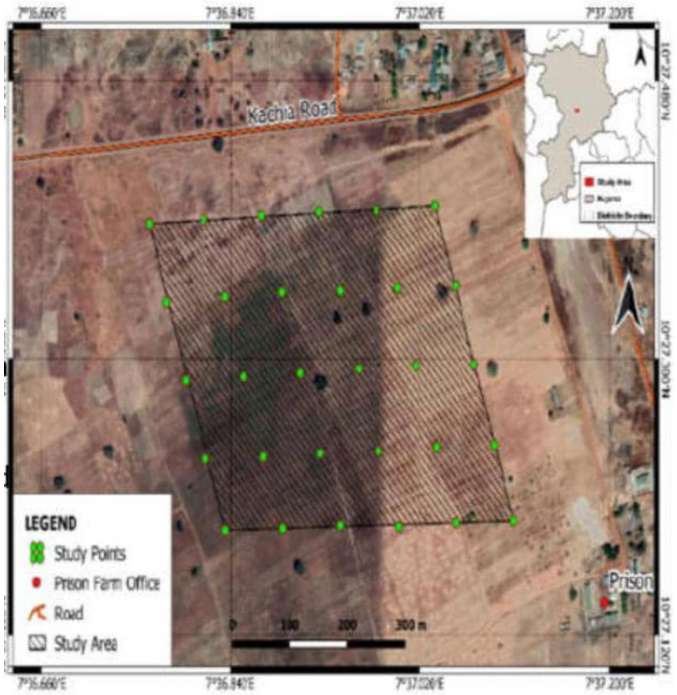

Figure 5: Google map of the study area showing the profile lines

Table 1: Coordinates Of Profile Locations

Profile line no	Coordinates
1	10° 30′ 21.2″ N, 07° 33′ 23.4″ E - 10°30′ 23.3″N, 07° 33′ 28.4″E
2	10° 29′08.4″N, 07° 33′ 23.4″E - 10°29′ 05.8″ N, 07° 32′38.6″E
3	10° 28′42.4″N, 07° 32 25.9″ E - 10°28′ 45. 9″N, 07° 32′ 28.7″E
4	10° 25′ 17.3″ N, 07° 30′ 38.9″E - 10°25′ 15.1″N, 07° 30′ 35.0″E
5	10° 23′ 42.6″N, 07° 28′ 58.3″E - 10°23′ 39.1″N, 07° 28′ 54.1″E

The recorded data were then processed using ReflexW software, version 10.4. Processing steps included visual inspection of raw data, noise filtering, and enhancement of signal quality before picking first arrivals (Yusoh et al., 2018). Figure6(a) shows the raw SRT before processing and Figure6(b) is the processed plot at shot point 50 m before picking the first arrival. First-arrival times were manually picked for each trace, and travel-time tomography was applied to generate 2D seismic velocity models of the subsurface. The velocity models were interpreted to distinguish between various subsurface layers. Zones with lower seismic velocities were inferred to represent weathered or saturated formations, potentially indicative of aquifer zones, while higher velocity zones corresponded to compact or dry bedrock (Akingboye, 2018). These interpretations were supported by correlating the seismic results with any available borehole data and surface geological observations, enhancing the reliability of subsurface characterization.

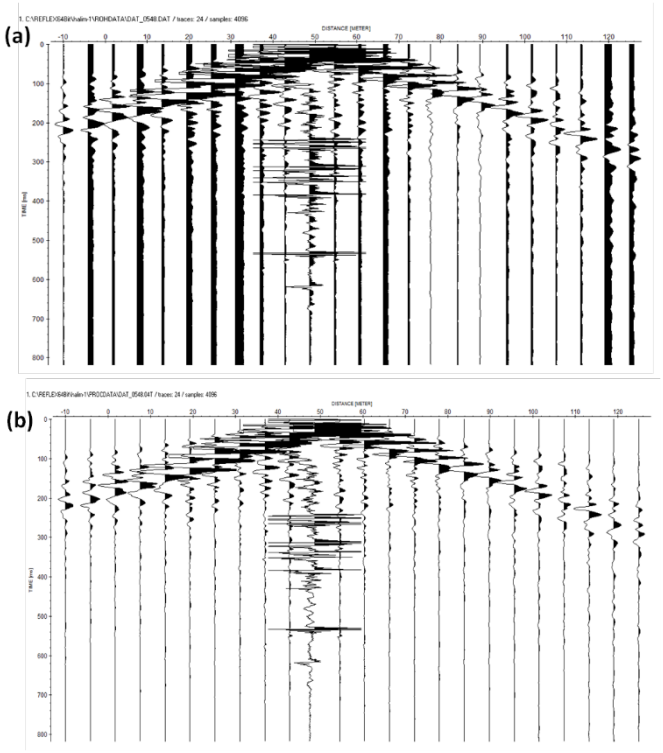

Figure 6: (a) Raw Seismic Refraction Tomography at 50 m (b) Processed Seismic Refraction Tomography

3.2.2. ERT

The Electrical Resistivity Tomography (ERT) survey was carried out using a computer-controlled resistivity imaging system comprising the ABEM Terrameter SAS 4000 and the ES 464 electrode selector. A total of 41 stainless steel electrodes connected via multi-core cables were deployed along each survey line, with 5 m spacing. The data acquisition process was managed using the RESIST software, which facilitated automatic verification of electrode connectivity and grounding before each measurement began. Signal averaging was employed to enhance data quality, and electrode tests were conducted to ensure proper ground contact, minimizing the possibility of measurement failure due to poor connectivity or battery issues. The measurement protocol was executed automatically, with the system operating in a multi-electrode mode to inject current and measure resulting potential differences, enabling the detection of subsurface resistivity contrasts. Raw resistivity data were processed using the RES2DINV software, which applies a 2D smoothness-constrained least-squares inversion algorithm to generate true resistivity models from the measured apparent resistivity values. The inversion corrects for geometric distortions and provides a resistivity cross-section that reflects actual subsurface conditions. The forward problem was solved using a finite difference method, and the inversion was iterated until a minimum error between calculated and measured apparent resistivities was achieved. The resulting resistivity sections were interpreted to delineate aquifer zones based on resistivity contrasts associated with variations in lithology, moisture content, and degree of weathering. Low resistivity values typically indicated water-saturated or clayey materials, while higher values were associated with dry, compacted, or crystalline basement rocks. The processed models were further supported by geological knowledge of the study area to ensure accurate interpretation of subsurface hydrogeological structures.

4. Results

4.1. SRT

The 2D seismic refraction data acquired across six profiles in the MarabanRido area were processed and inverted using a three-layer model to generate velocity tomograms. The Blue–Grey–Red (BGR) and Rainbow color palettes (Fig. 7) were employed for visualization, with blue representing lower velocities (saturated zones or topsoil) and red/violet representing higher velocities (denser, unweathered basement). For the BGR model of the first profile, three distinct geologic layers were interpreted based on seismic velocity values. The first layer (0–10 m

depth), with velocities ranging from <457 to 650 m/s, is attributed to topsoil and unconsolidated materials such as laterite and dry sand. The second layer, ranging from 660 to approximately 1150 m/s, represents the weathered basement, including compacted sandy/clayey materials and highly to moderately weathered granite. The third layer, showing velocities above 1200 m/s, is interpreted as fresh crystalline basement rock, composed of quartz and gneiss. The rainbow palette model (Fig. 7b) shows a more intricate differentiation, where the geological transitions are better defined. The color changes from yellow to red and then purple indicate increasing density of the subsurface geological formations.

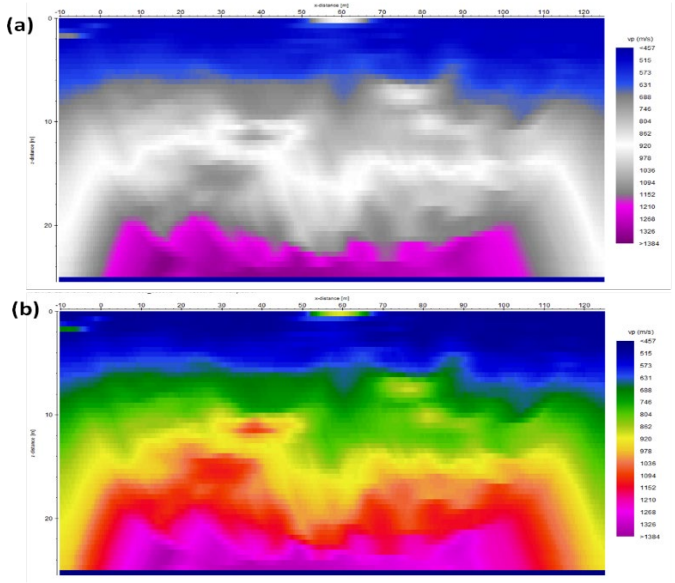

Figure 7: Velocity models using (a) Blue_Grey_Red palette (b) Rainbow palette for profile 1

The tomography model for profile 2 (Fig. 8) can be divided into three main layers of overburden, weathered andfresh basement based on the velocity classifications from standard values.The first layer in blue colour (between 0 and 10 m in depth) has a maximum velocity of 818 m/s corresponds to top soil (overburden) whichcould be laterite and dry sand. The average thickness of the overburden is about 8 m, which is similar to profile 1. The second layer is characterized by higher seismic velocities (from about 959 m/s to about 2089 m/s) with thickness ranging from 10m to 20m. This layer istypical of sandy clay, clay and saturated,fine to medium and coarse soil. This layer is considered the weatheredbasement. The third layer which is violet or purpleincolour shows an increase of seismic wave velocity (from 2370 m/s andabove), which could be attributed to the fresh crystalline basement rocks.The average depth to the basement is about 20 m. This implies that the average thickness of the weathered basement is about 12 m. The rainbow palette model (Fig. 8b) shows the intrusion of layer 2 (yellow color) into the underlying fresh basement, which is possibly a fracture zone.

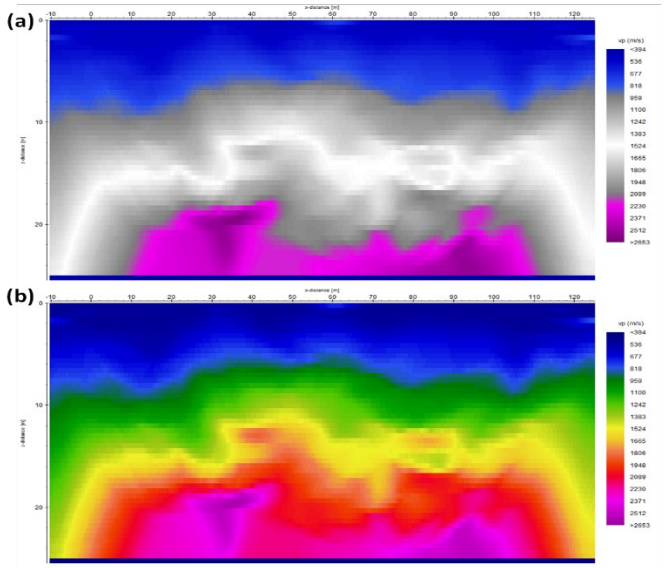

Figure 8: Velocity models using (a) Blue_Grey_Red palette (b) Rainbow palette for profile 2

Profile 3 has a maximum velocity of 794 m/s for it first layer attributed to topsoil. Layer 2, with a velocity range of 925 m/s to 1971 m/s, is interpreted as a combination of dry sand and weathered basement materials. Specifically, the lower velocity portion (925 m/s to around 1971m/s) likely represents highly weathered rock, while the higher velocity range (above 2102 m/s) may indicate moderately weathered granite. The average thickness of the overburden, which also represents the depth to the refractor, is about 8 m. The average depth to the basement is approximately 35 m, implying that the average thickness of the weathered basement is about 27 m.

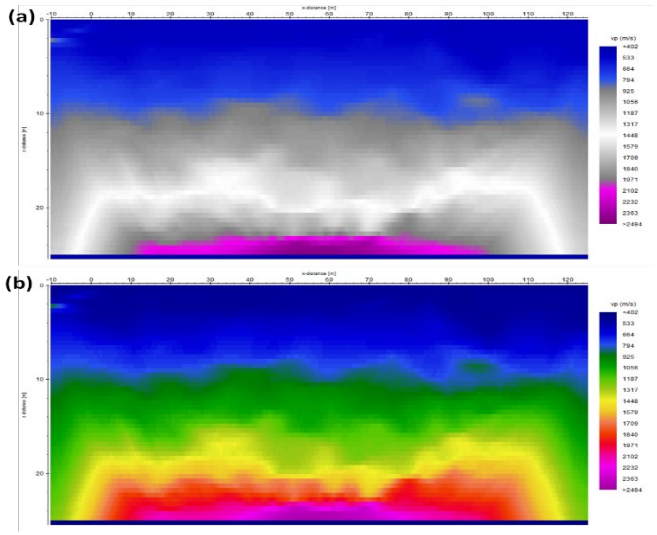

Figure 9: Velocity models using (a) Blue_Grey_Red palette (b) Rainbow palette for profile 3

The first layer for profile 4 (Fig. 10) has a velocity range of 362 m/s to 967 m/s, which is attributed to topsoil and possibly loose, unconsolidated materials with depth of 15m. The second layer, with a velocity range of 1102 m/s to 2584 m/s, is interpreted as a transition zone consisting of compacted sand and weathered basement rock. The lower end of this range (1102 m/s to around 2584 m/s with depth of 16 - 40m) likely represents compacted sandy or silty materials, while the higher velocities suggest moderately weathered basement rock. The thickness of the overburden, representing the depth to the top of the refractor, is about 15 m. The average depth to the basement is between 34 m and 40 m, indicating that the weathered basement zone has a thickness ranging from approximately 19 m to 25 m. The third layer, with a velocity range of 2769 m/s to 3324 m/s, is interpreted as the fresh basement. Profile 5 depicts a similar velocity model as profile 4. The BGR palette model (Fig. 11a) show 3 distinct layers with velocity ranges of 0- 897 m/s, 1196-3588m/s, and 3588 – 4785 m/s denoting the top unconsolidated lateritic soil, weathered basement rocks, and fresh crystalline basement, respectively, with average thicknesses of 8, 17 and 30 m. The rainbow palette for profile 5 (Fig. 11b) indicate the presence of an igneous intrusion or unweathered basement material within layer 2 at point 80 to 90 m. At point 30 m, a possible fracture is discernible within the fresh basement, which could serve as a potential aquiferous zone.

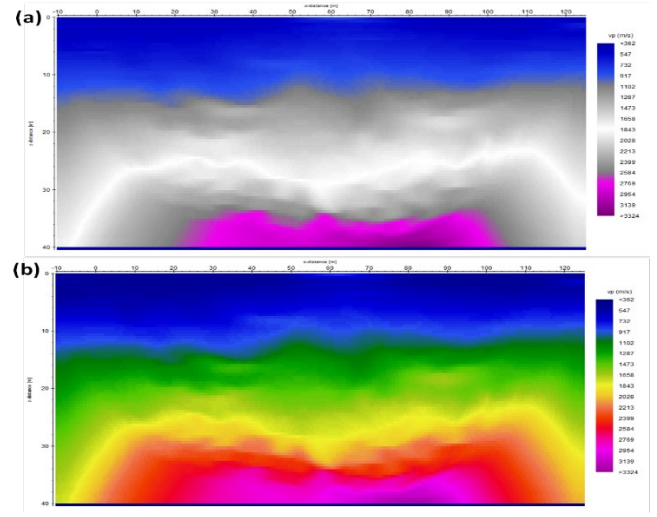

Figure 10: Velocity models using (a) Blue_Grey_Red palette (b) Rainbow palette for profile 4

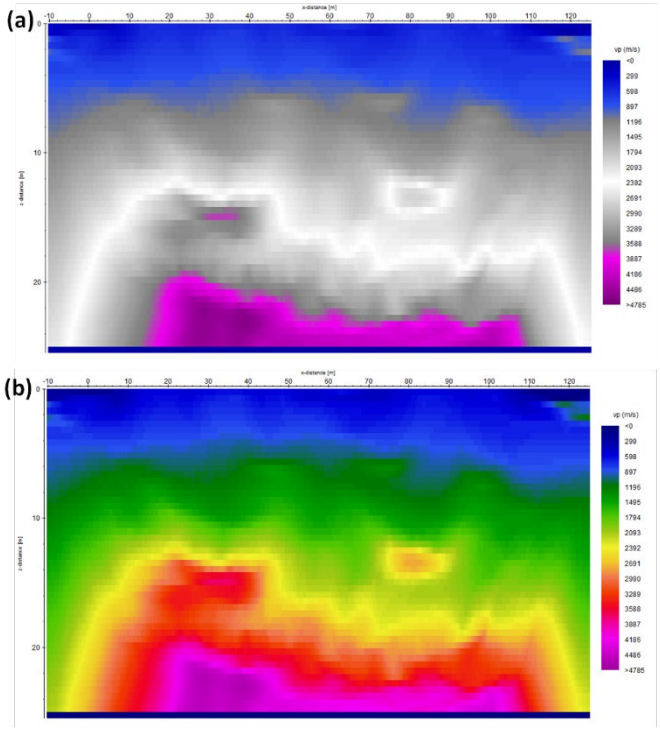

Figure 11: Velocity models using (a) Blue_Grey_Red palette (b) Rainbow palette for profile 5

4.2 ERT

The results of 2D inversion are shown in figures 12 to 16. The images show plots of the apparent resistivity with depth, which is then contoured (commonly krigged) using the software program. The pseudosection presents color contoured image that displays the distribution of apparent resistivity values and associated gradients across the area of interest.In order to convert the apparent resistivity data to true resistivity, the data are inverted. The ERI profile shows the measured apparent resistivity pseudosection at the top, followed by a calculated apparent resistivity pseudosection, and resulting in the inverted true resistivity 2D section at the bottom for each profile.The numbers presented at the bottom of the inverted section display goodness of fit criteria used to assess the accuracy of the calculated resistivity model. In addition, the surface elevations are included in the final model, accounting for variations in measurement geometry due to changing topography.

For profile 1 (Fig. 12), the upper part of the layer reveals resistive materials at the top layer. The resistivity values range from 45.1-96.9 Ωm with a thickness of about 6.5 m. The top layer (lateritic clay/sandy clay) is underlain by a weathered basement, which has a depth range of 3 -10.5 m with resistivity values between 200 - 447 Ωm to 854Ωm. The high resistivity values (200 – 959Ωm) are seen at the depth range above 19.5m. a resistive material with a resistivity of about 2058 ohm meter is observed at a depth of about 20.1m, this layer is underlain by a resistive layer with a resistivity range between 4418 – 9486Ωm.

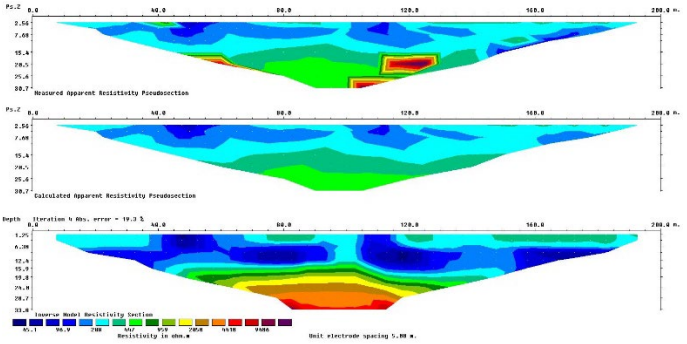

Figure 12: Resistivity cross section for profile 1

In Profile 2 (Fig. 13), the upper part of the layer reveals conductive materials at the top layer. The resistivity values range from 37.3-82.0 Ωm with a thickness of about 2 m. The top layer (lateritic clay/sandy clay) is underlain by a weathered basement, which has a depth range of 2-7.8 m with resistivity values between 179 - 391 Ωm. The lower part of the layer reveals high resistive (1865Ωm) rocks with a thickness of about 2 m to the eastern part of the section. This section is underlain by a fresh basement, with a depth of above 12.5m and a resistivity range of 4072 – 8894 Ωm.

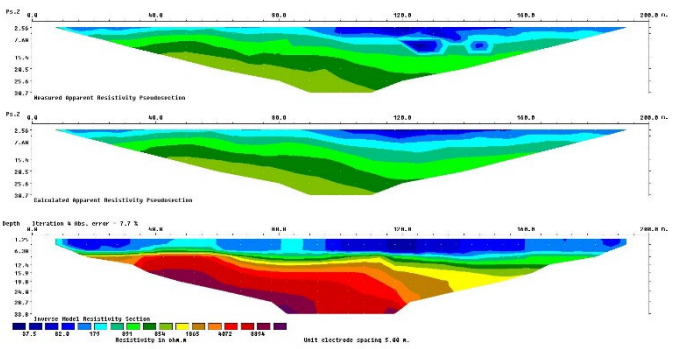

Figure 13: Resistivity cross-section for Profile 2

Profile 3 (Fig. 14) also reveals resistive materials at the top layer. The resistivity values range from 1581-2447Ωm with a thickness of about 2 m and depth of 7.1m. The top layer is underlain by a weathered basement, which has resistivity values between 276-427 Ωm, with a depth range of 9.1-13.8m. This was absent between lateral distance of 160-200 m where the resistivity of the materials ranges between 1581-2447 Ωm, with a resistive material serving as a demarcation between the top layer and the weathered basement with a resistivity of about 1022 Ωm.

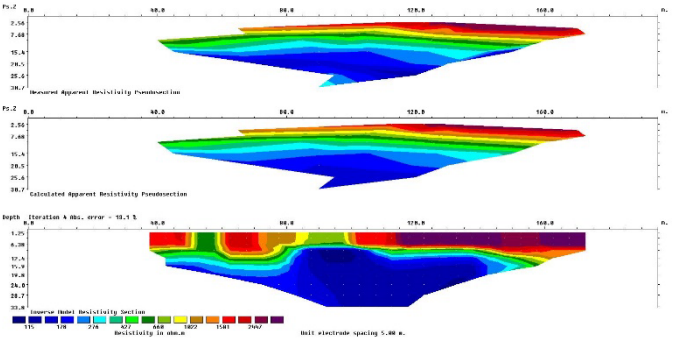

Figure 14: Resistivity cross-section for profile 3

In Profile 4 (Fig. 15), the upper part of the layer reveals resistive materials at the top layer in to the SW part of the section, the resistivity values range from 666-1108Ωm with a thickness of about 2.5 m. The weather basement is underlain with a conductive layer with a resistivity range of 86.5 – 145 Ωm, with a depth range of about 12.4m - 33.4m, and a thickness of about 20.6m. (fig.3j). At alateral distance of 8.5 -87 m and depth of about 6.7 m, theobserved areas with moderate resistivity of 400Ωm serve as a sharp demarcation between the top high resistivity layerand underlying relatively lower resistivity zone.

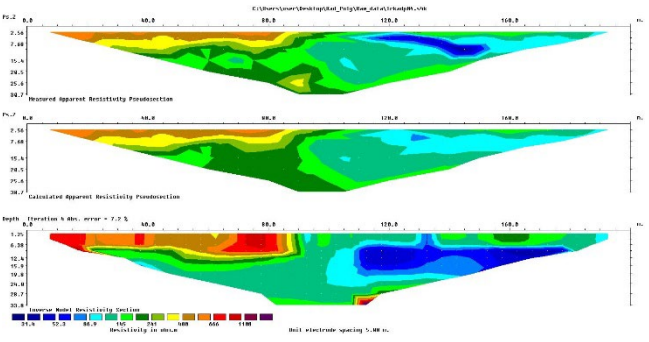

Figure 15: Resistivity cross-section for profile 4

In Profile 5 (Fig. 16), the upper part of the layer reveals resistive materials at the top layer. The resistivity values range from 432-733, Ωm with a thickness of about 2 m. Observed at a lateral distance of about 45 – 52 m is the presence of a highly resistive (1243Ωm) material, possibly a granitic intrusion. The top layer (lateritic clay/sandy clay) is underlain by a weathered basement, which has a depth of about 12.4m, with resistivity values between 88.6 and 432 Ωm. The third layer is characterized by resistive rock materials with values ranging between 1243 and 3576 Ωm at a depth range of 28-33.8m.This implies that the subsurface contains resistive materials. The upper part of the layer reveals moderate resistive materials at the top layer in this profile.

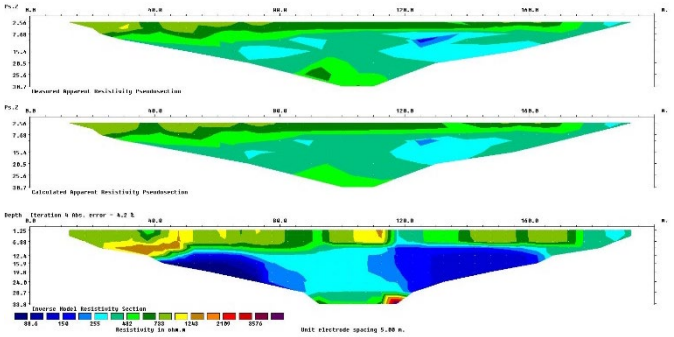

Figure 16: Resistivity cross-section for profile 5

5. Discussion

The integration of SRT and ERT in this study has effectively addressed the need for a more comprehensive and accurate delineation of aquifer zones around MarabanRido, Kaduna NW. This dual geophysical approach draws directly from the findings and assertions established in the literature review, which emphasizes the limitations of using a single geophysical method in complex geological terrains. This research ERT are efficient for characterizing subsurface materials and detecting hydrogeological boundaries (Subash et al., 2010). This was strongly validated by this study, where the ERT profiles successfully identified weathered basement zones, lateritic/sandy clay layers, and fresh basement rocks with varying resistivity values across the profiles. These zones are critically important in groundwater prospecting because the weathered and fractured zones often act as the main aquifer units. Furthermore, consistent with the complementary nature of SRT and ERT methods was evident (Kirsch, 2019; Adepelumi et al., 2018). The findings align with who observed improved detection of aquifer boundaries when both seismic and resistivity methods were jointly applied in basement complex terrains (Parisa et al., 2021). While SRT provided high resolution seismic velocity models that mapped subsurface mechanical contrasts particularly depth to refractor and basement structure, ERT offered insights into electrical resistivity, which is more sensitive to moisture content, porosity, and lithology.

In particular, profiles from the SRT survey revealed velocity layering consistent with lithologic variations, from topsoil (low velocities), to weathered basement (moderate velocities), to fresh crystalline basement (high velocities). Velocity, depth and thickness variations across the five profiles are presented in Table 2.All profiles reveal a consistent topsoil/unconsolidated cover and weathered basement fresh crystalline basement architecture. Basement undulations produce localized depressions (notably on P1, P2, P5) that correspond to thickened weathered zones, whereas P3 and P4 exhibit regionally thicker weathered zones with deeper basement on P4. The fresh basement could be of crystalline quartz-gneiss, expressed by velocities ≥ 2700–3300 m/s.Profile 3 presented a layered model with topsoil velocities up to 794 m/s, increasing to over 2000 m/s in the deeper sections, suggesting the presence of weathered and moderately weathered basement rocks.

For most profiles, the overburden thickness averaged 8–15 m, while the depth to fresh basement ranged between 20 and 40 m, implying weathered basement zones of 12–27 m thickness. Profile 3, for instance, showed a significant weathered zone up to 27 m thick, with seismic velocities indicating a transition from dry sand to moderately weathered granite. Similarly, profile 4 exhibited a broader range of basement depths (34–40 m), with the fresh basement characterized by velocities between 2769 and 3324 m/s. A notable feature across profiles 1, 2, and 5 is a syncline-like depression observed between 50 and 90 m along the profile, with basement velocities dipping in this section. This structural depression likely acts as a groundwater reservoir, making it a promising site for borehole drilling. The absence of faults, sinkholes, or unstable formations within the profiles further supports the suitability of the area for groundwater abstraction and civil engineering applications.

Table 2: Velocity, depth and thickness variations across the five profiles in the research area

S/N	P1	P2	P3	P4	P5	Interpretation
Layer 1						Surficial cover/top soil(overburden), comprising lateritic unconsolidated loose sediments
Velocity (m/s)	<457 – 631	<394 – 818	402 – 794	<362 – 917	0-897	
Depth (m)	8	8	10	15	8	
Thickness (m)	8	8	10	15	8	
Layer 2						Weathered basement rock. The porous nature of this sandy layer and the sealing properties of the clayey and underlying fresh basement allows for the formation of an aquifer
Velocity (m/s)	688-1094	959 – 1948	925 – 1971	1102 – 2584	1196 - 3588	
Depth (m)	30	28	25	40	25	
Thickness (m)	22	20	15	25	17	
Aquifer thickness	4	2	20	8	2	
Layer 3						Fresh crystalline basement rock
Velocity (m/s)	1152 - 1384	2089 – 2653	2102 – 2494	2769 – 3324	3588 – 4785	
Depth (m)	18	18	23	40	30	
Thickness (m)	4	10	2	15	13	
Depressed zone						A gentle synclinal depression that possibly hosts a thick section of weathered sediments overlying the fresh basement
Thickness (m)	50 – 90	50 – 90	-	50 – 60	50 – 90	
Transition zone (Velocity (m/s))						
Zone between layers 1 and 2 (m/s)	631	818	794	917	886	The zone between the unconsolidated sediments and underlying weathered zone, possibly a consolidated clayey layer
Zone between layers 2 and 3 (m/s)	920	1524	1448	1843	2591	Zone between weathered layer and underlying fresh basement

Importantly, emphasized the benefit of combining multiple geophysical methods for enhanced resolution and overcoming interpretational ambiguities (Ahmed et al., 2014). This research substantiates that claim through the successful correlation of velocity and resistivity data, particularly in identifying aquifer bearing depressions and structural features which were interpreted from seismic models (e.g., between 50–60 m along Profile 1). The findings indicate significant groundwater potential in zones characterized by moderate seismic velocities (900–2100 m/s), resistivity values ranging from 88–450 Ωm, layer thickness of 12 – 25 m for weathered basement, and absence of active faulting or sinkholes that supports stability. Such zones are interpreted as weathered or fractured basement aquifers, consistent with the model of secondary porosity systems typical in Precambrian basement terrains. The ERT results further supported the seismic interpretations by revealing resistivity contrasts that correspond with topsoil, weathered basement, and fresh basement rock. Particularly, profiles 1, 2, and 4 indicate depressions in the basement, forming potential groundwater aquifer zones, a concept supported in identifying depression structures as water collection zones by (Karimi, 2012).Low to moderate resistivity values (37–447 Ωm) in profiles 1 and 2 at shallow depths (0–10 m) suggest the presence of weathered basement and lateritic/sandy clay, which may serve as water-bearing formations. As observed in Table 3, profile 1 showed resistivity values of 45–96.9 Ωm in the topsoil layer, 200–854 Ωm in the weathered basement, and >2058 Ωm in the fresh basement. Such high resistivity zones indicate non aquiferous crystalline rocks, while moderate resistivity zones correlate with weathered or fractured materials with groundwater storage potential.Thin resistive layers (666–2447 Ωm) near the surface at ERT profile 3 may represent lateritic hardpan or crystalline rocks, which disrupt surface recharge and hinder access to groundwater. Profiles 3 and 4 showed alternating resistive and

conductive layers, with moderately conductive zones (86.5–427 Ωm) between 7.1–33.4 m depth, indicating weathered basement with potential for groundwater storage.Profile 5 showed similar low to moderate resistivity values (88–432 Ωm) down to 24 m, implying aquiferous potential, though high resistivity values (>2000 Ωm) at deeper levels reflect the presence of fresh basement rock, limiting groundwater availability. Additionally, the presence of lateritic hardpans and localized resistive anomalies (e.g., 1243 Ωm at 2 m in profile 5) may indicate igneous intrusions that could impact groundwater recharge and flow, either as flow barriers or redirectors, affirming the need for geophysical integration to understand these subsurface complexities. The differentiated subsurface geology based on the geophysical methods is depicted in Figure 17.

Table 3: Showing Resistivity, depth and thickness of layers across the five profiles in the research area

Profiles	P1	P2	P3	P4	P5	Interpretation
Layer 1						Thin lateritic clay/sandy cover (~6.5 m) overlying a moderately resistive weathered zone, with the exception of profile 3. Profile 3 comprises resistive crystalline rock at the surface
Resistivity(Ω m)	45.1 - 96.9	37.3 - 82.0	158 1- 244 7	50 - 300 , 666 - 110 8	432 -73	
Depth(m)	6.5	4	7.1	12	7.5	
Thickness(m)	6.5	4	7.1	12	7.5	
Layer 2						Conductive weathered/fractured zone (179–391 Ω·m, ~5 m thick). Moderate aquifer potential within L2; water storage possible but yield may be modest.
Resistivity(Ωm)	447 - 959	179 - 391	276 - 427	86. 5- 145	88.6 - 432	
Depth(m)	15	9.0	13.8	30. 0	25.5	
Thickness(m)	13	5	6.7	18	18	
Layer 3						Highly resistive fresh basement, with the exception of profile 3.
Resistivity(Ω m)	441 8- 948 6	407 3- 889 4	115 - 178 Ω	400	124 8- 357 6	
Depth(m)	30.8	30.0	31.0	30. 0	33.8	
Thickness(m)	17.3	25	24.3	12	5.8	

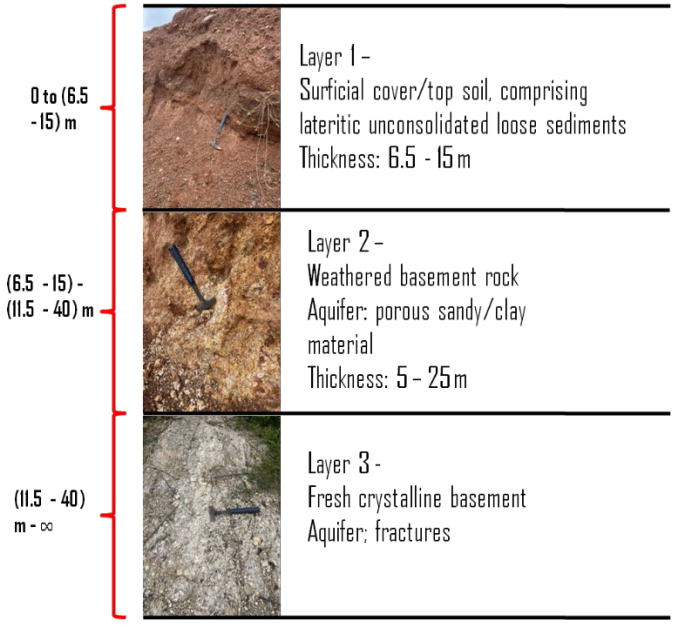

Figure 17: Variations in the subsurface geology with depth

The novelty of this research lies in the site specific integration and detailed correlation of SRT and ERT datasets to resolve hydrogeological complexities within a crystalline basement terrain in Northwestern Nigeria. Unlike previous studies that often relied on single method interpretations, this study combines mechanical (velocity) and electrical (resistivity) signatures for enhanced interpretation accuracy. The approach identifies and characterizes aquiferous zones within basement depressions, which had not been previously documented in detail around MarabanRido. The combined methods accurately differentiates between saturated weathered basement, hardpans, and fresh basement with higher confidence using cross validation from two methods, and confirms the absence of fault related groundwater conduits or hazardous subsurface features, thereby informing both hydrogeological and engineering applications. This study provides a template for integrating ERT and SRT in similar basement complex terrains with minimal borehole data.

Given the results and their alignment with literature, future groundwater exploration should target zones of moderate velocity and moderate resistivity, typically indicative of saturated weathered fractured basement. Borehole drilling should avoid highly resistive and high velocity zones, which likely represent unfractured crystalline basement. Areas like zones with depression in profile 1 (50–60 m) represent prime targets for viable groundwater abstraction. The integrated method should be applied in urban planning, as it supports decisions related to foundation integrity and liquefaction potential.

6. Conclusion

The overall results provide a reliable delineation of aquifer-bearing zones, weathered bedrock, and the underlying fresh basement, making the both method effective for hydrogeological assessment in the complex basement terrain of MarabanRido. The velocity gradients suggest that the water table in the MarabanRido area lies at approximately 10–15 m depth, with no evidence of shallow water-saturated zones near the surface. On the other hand, ERT area revealed significant subsurface resistivity variations useful for delineating aquifer zones. Overall, the ERT results identify potential zones for groundwater abstraction, particularly within weathered and fractured basement layers. In contrast, the SRT clearly delineated the subsurface geology based on density variations, indicating the presence of structures and identifying transitions from surface unconsolidated soil to the crystalline basement rocks with depth.

References

Adegbuyi, Abdelgowad, A. M., El-Haddad, A. E., Aglan, M. I., et al., 2025. Seismic refraction investigation of the shallow bedrock in New Qena City, Eastern Desert, Egypt.Scientific Reports, 15, Pp. 2646. https://doi.org/10.1038/s41598-025-85949-5

Adedibu, S. K., and Ogunyele, A. C.2019. Insight into seismic refraction and electrical resistivity tomography techniques in subsurface investigations.

Aizebeokhai, A., Ogungbade, O., and Oyeyemi, K., 2018.Geoelectrical resistivity data set for characterising crystalline basement aquifers in Basiri, Ado-Ekiti, southwestern Nigeria. Data in Brief, 19, 10.1016/j.dib.2018.05.091

Aizebeokhai, A., Oni, A., and Oyeyemi, K., 2018, December 11. Groundwater exploration in crystalline basement complex using seismic refraction and electrical resistivity tomography: Case study of Olomore, Abeokuta, southwestern Nigeria. Authorea. https://doi.org/10.1002/essoar.10500244.1

Akindeji, F., 2020.Integrated geophysical investigation of aquifer and its groundwater potential in phases 1 and 2, Federal University Oye-Ekiti, south-western basement complex of Nigeria. Modeling Earth Systems and Environment, 6, Pp. 1747–1760. https://doi.org/10.1007/s40808-020-00785-y

Akingboye, A., and Ogunyele, A., 2019.Insight into seismic refraction and electrical resistivity tomography techniques in subsurface investigations.Rudarsko-Geološko-NaftniZbornik, 34(1), Pp. 93–111. https://doi.org/10.17794/rgn.2019.1.9

Ali, A., Ben-Awuah, J., Saad, R., and Andriamihaja, S., 2017. Combined use of 2D electrical resistivity and seismic refraction in hydrogeophysical exploration. Petroleum and Coal, 59, Pp. 231–239.

Apenna, V., Loperte, A., Perrone, A., and Telesca, L., 2009.2D electrical resistivity tomography for investigating recent activation landslides in Basilicata Region (Southern Italy). Annals of Geophysics, 51(1), Pp. 275–285.

Fatihu, S., Maniyunda, L. M., Adegoke, K. A., and Anumah, A., 2021. Evaluating quality of soils formed on basement complex rocks in Kaduna State, northern Guinea savanna of Nigeria. Environmental Monitoring and Assessment, 193, 572. https://doi.org/10.1007/s10661-021-09157-0

Gladys Maju-Oyovwikowhe, E., Uwa-Igbinoba, E., and Alile, O. M., 2024. Integrated geophysical techniques for subsurface characterization and groundwater assessment: A case study from the University of Benin, Nigeria. In Advances in Groundwater Research.IntechOpen. https://doi.org/10.5772/intechopen.1006853

Google Earth. 2025. Satellite imagery of study area.Google. https://earth.google.com

Griffiths, D.H., and Barker, R.D., 1993. Two-Dimensional Resistivity Imaging and Modeling in Areas of Complex Geology. Journal of Applied Geophysics, 29, Pp. 21-26.

http://dx.doi.org/10.1016/0926-9851(93)90005-J

IOP Conference Series: Earth and Environmental Science, 23, 012013. https://doi.org/10.1088/1755-1315/23/1/012013

Ismail, Nur and Saad, Rosli and Nordiana, M.M., 2013. Applying the Seismic Refraction Tomography for Site Characterization. APCBEE Procedia. 5. Pp.227–231. 10.1016/j.apcbee.2013.05.039.

Karimi, H., 2012. Hydrogeology of karsticarea.In Hydrogeology. A Global Perspective. Intech Open. https://doi.org/10.5772/28351

Kirsch, R., 2009.Groundwater geophysics.Springer. https://doi.org/10.1007/978-3-540-88405-7_16

Mahmud, M. L., Holt, R., Hickey, C., Davidson, G., Wodajo, L., Bakhtiari Rad, P., Samad, M. A., Buskes, E., and Mahmud, M. I., 2022. Groundwater aquifer delineation using electrical resistivity tomography and vertical electrical sounding.Geological Society of America Abstracts with Programs, 54(6). https://doi.org/10.1130/abs/2022AM-382664

Nisa, A., Saad, R., and Nordiana, M. M., 2013.Integration of seismic refraction and 2D electrical resistivity in locating geological contact.Journal of Geology, 3(2B).

Parisa, I., Tian, G., Hadiloo, S., El-Raouf, A., 2021. Application of combined electrical resistivity tomography (ERT) and seismic refraction tomography (SRT) methods to investigate Xiaoshan District landslide site: Hangzhou, China, Journal of Applied Geophysics,Volume 184, 2021, 104236,https://doi.org/10.1016/j.jappgeo.2020.104236.

Parkman International, and Parkman Nigeria Limited. 1997. State-wide water resources master plan: Kaduna State.

Salako, A. O., and Adepelumi, A. A., 2018.Aquifer classification and characterization.InHydrogeophysics and groundwater exploration, Pp. 11–31.Springer. https://doi.org/10.1007/978-3-319-60095-7_2

Subash Chandra, Dewandel, B., Dutta, S., and Ahmed, S., 2010. Geophysical model of geological discontinuities in a granitic aquifer: Analyzing small-scale variability of electrical resistivity for groundwater occurrences. Journal of Applied Geophysics, 71(4), Pp. 137–148. https://doi.org/10.1016/j.jappgeo.2010.06.003

Yadav, G. S., and Abolfazli, H., 1998.Geoelectrical soundings and their relationship to hydraulic parameters in semiarid regions of Jalore, northwestern India. Journal of Applied Geophysics, 39(1), Pp. 35–51. https://doi.org/10.1016/S0926-9851(98)00003-2

Young, B., 1962. Report on the basement complex geology of the eastern half of the 1:100,000 sheet 189, Kurra; Unpublished GSN Report No. 1323. Geological Survey of Nigeria.

Yusoh, R., Saad, R., Saidin, M., Muhammad, S.B., 2018. Anda, S.T. IOP Publishing. Journal of Physics: Conference Series: Vol. 995. International Seminar on Mathematics and Physics in Sciences and Technology 2017 (ISMAP 2017), Pp. 28–29 October 2017, Hotel Katerina, Malaysia.IOP Publishing. https://doi.org/10.1088/1742-6596/995/1/